AIAA 13st Space Planes and Hypersonic Systems and Technologies Conference,
Capua, Italy, 16 - 20 May 2005

AIAA-2005-3294

The Hypersonic Flight Experiment SHEFEX

Th. Eggers, J.M.A. Longo

DLR, Institute of Aerodynamics and Flow Technology, Lilienthalplatz 7, 38108 Braunschweig, Germany

M. Hörschgen, A. Stamminger

DLR, Mobile Rocket Base MORABA, 82234 Weßling

Abstract

The purpose of the SHarp Edge Flight EXperiment SHEFEX is the investigation of possible new shapes for future launcher or reentry vehicles [1]. The main focus is the improvement of common space vehicle shapes by application of facetted surfaces and sharp edges. The experiment will enable the time accurate investigation of the flow effects and their structural answer during the hypersonic flight from 90 km down to an altitude of 20 km. The project, being performed under responsibility of the German Aerospace Center (DLR) is scheduled to fly on top of a two-stage solid propellant sounding rocket for October 2005. The paper decribes the overall philosophy of the project and gives a survey of the aerodynamic and aerothermodynamic as well as the configurational layout of the experimental vehicle.

1. Introduction

Early in the fifties few small hypersonic wind tunnels had been used almost entirely for fluid mechanics studies but they were unable to simulate neither the high temperatures nor the high Reynolds number of flight. Because of strongly interacting flow fields, viscous interactions with strong shocks, and possible real gas effects, it was generally feared that testing in these limited wind tunnels would not produce valid results. It was expected that the first hypersonic vehicles would reveal large discrepancies between flight and ground test data, as was the case of the X-15, US-Orbiter, Russian-Buran and Japan-HST. Fifty years later and with some progress within the space community in designing, building and flying hypersonic gliding vehicles like e.g. the ARD capsule (Fig. 1) is possible. But, the fatal flight of the Columbia in 2003 again showed the severity of the hypersonic environment. Indeed, hypersonic systems are complex, difficult to design and expensive to build due to a lack of physical understanding on the involved flow regimes and a lack of data for design. Although in each decade considerable energy is spent designing new concepts and developing the technology base required to support them, no aircraft capable of flying at Mach 10 or higher has been built.

It is obvious, that current space transportation systems do not enable routine low-cost operations. In order to improve the reliability of accessing space, e.g. problems related to vehicle servicing and refurnishing, must be hardly simplified and the time required for a design cycle has to be drastically reduced. The required technological developments are directly associated to the technological progress of the three disciplines: Aero(thermo)dynamics, Propulsion, Structures and Materials. A close interaction of these three disciplines, as well as the optimal use of all technical potentialities is necessary for a drastic reduction of design times, improved vehicle performance and operations.

Due to the complexity of the problem computational or “virtual“ vehicle design and qualification is the strategic tool which one day will enable to reduce dramatically the design and development time required for new vehicles. But a computational design is based on mathematical models which require verification and validation for establishing credibility. To accomplish its mission, physical modelling strongly requires good ground facilities and flight data to be used for code validation and when necessary code calibration too. Ground based facilities, the major source of flow data, are very important because they allow a better understanding of the flow physics but in flight-measurement constitutes the only way to obtain data for prediction tools validation and calibration under real conditions and therefore, they are irreplaceable for physical modelling [2]. One of the big mistakes of the last 25 years has been the strong coupling of the progress in hypersonic physics with new operational systems developments instead of use less complex systems like sounding rockets as test bed for new technological concepts or for simple gathering of flight data which are representative of the real hypersonic environments. Many X-programs, such as Hermes, the X-30, Sänger, X-33, X-34 and the X-38 have failed, in

some cases short before the flight test that would produce the data, so necessary to advance our understanding of the hypersonic environment and how to design vehicles that would survive in that environment. Those failures occured partially due to economical reasons and partially due to the technological challenges associated with the projects, being the first cause also closely related to the second one. Sounding rockets may be the way of access to a certain type of "sky based facility" (in analogy to the ground based facilities) but extremely less expensive and less risky than the so-called X-vehicles. Emerging examples of such strategy are the SOAREX experiment from NASA [3], to test future flight vehicle concepts and the HyShot experiment of the University of Queensland [4], to test supersonic combustion. At DLR this approach is being adopted defining the SHEFEX project as the pathfinder experiment.

2. Definition of the Experiment

The objective of the SHEFEX experiment is the exploration of a facetted TPS concept and the assessment of the potential of sharp edged configurations applying the three points strategy: numerics - ground based facilities - flight experiment (Fig. 2). The motivation is neither to perform a re-entry experiment nor to fly at the thermal boundary of modern high temperature materials but to provide flight evidences that the temperature peaks at the edges of the ceramic-composite panels are lower than those predicted based on a radiation equilibrium hypothesis.

From the structural point of view fabrication, inspection / repair and payload displacement costs are the three major elements determining the TPS cost per unit of each system [5]. Fabrication represents the cost for purchase and installation of the TPS. Inspection / repair, or maintenance / servicing, represents the cost for re-flight certification. Payload displacement represents the payload mass displaced by the TPS and is the dominating parameter. An increase in TPS mass displaces payload for the life cycle of the vehicle, and significantly increases the payload delivery cost to and from orbit, since TPS total mass may be equivalent in some cases to the vehicle payload mass. Indeed, the mass and cost of a thermal protection system (TPS) heavily impact the economic performance of the vehicle: a 20 % increase in vehicle dry mass causes a 35 % increase in TPS mass. From a TPS-servicing point of view a crude analysis about the economic potential of a facetted TPS system has been obtained considering a hypothetical situation with a modern aerospace vehicle. The exercise consisted to look first into the aerodynamic impact which would have such kind of vehicle if its front section is covered by planar panels instead of a contoured ones. The numerical computation showed no major impact on the aerodynamic behavior of the vehicle (Fig. 4). Panels of 0.8 m maximum length have been considered to account for thermal expansion / contraction problems. To cover the front section of a vehicle like Phoenix almost 50 exact contoured panels are necessary, requiring also 50 manufacturing tools, or 70 flat panels requiring only one manufacturing tool. It turns out, that a saving in manufacturing cost of about 70% accompanied with a strong reduction in development time due to the simplicity of the design is possible. In addition, for the operation of four vehicles, the saving due to TPS inspection, simplicity in replacing and sealing allow another 40 to 50% on the system level.

From the aerodynamic point of view the design of a hypersonic vehicle is affected by finding a compromise between a vehicle being sharp enough to obtain acceptable aerodynamic and propulsion efficiency and blunt enough to reduce the aerodynamic heating. Therefore, during the 1990s the development of ceramic composite and ultra high temperature materials for thermal protection system applications led to a renewed interest on sharp edged configurations like e.g. the waverider concept DLR F8 [6], the DLR-ONERA project JAPHAR [7] or the lifting body concept HL-20 and the SHARP project, both from NASA [8], [9]. The current experiment SHEFEX is presented here.

Driven by the facetted concept, two main criteria have been used to define the aerodynamic shape of SHEFEX. It should have as much as possible facetted panels and it should represent as many as possible configuration details of space vehicles, like concave and convex chamfers and a sharp unswept leading edge. The experiment shall enable a detailed investigation of the flow effects and their structural answer during flight.

3. Introduction of the SHEFEX Mission

The SHEFEX launcher is a two-stage solid propellant sounding rocket system conceived primarily for ballistic microgravity experiments. The launch vehicle consists of a Brazilian S30 motor as first stage and an Improved Orion motor as second stage (Fig. 5). This motor combination has been launched successfully two times in basically the same rocket configuration. Between the facetted forebody and the second stage are two cylindrical modules which house the recovery system, the main electronics, the data acquisition devices, the power supply and the cold gas RCS (Fig. 6). During the ascent the facetted forebody is protected by an ogival nose cone.

The projected mission is schematically sketched in (Fig. 7). It is a suborbital flight mission started from Andoya (Norway). The first stage burns out after 28 sec and sep-

arates from the rest of the launcher at an altitude of 17 km. The second stage burns out after 56 sec at an altitude of 65 km. Since the facetted body has no control devices the second stage remains attached to the facetted body until the end of the experiment to provide flight stability through its fins (Fig. 6). At about 90 km, the nose cone separates and a cold gas RCS initiates the pointing maneuver. The apogee is reached at approx. 300 km. No yo-yo de-spinning maneuver is necessary since the RCS eliminates any remaining spin. The SHEFEX experiment starts at an altitude of 90 km and continues with almost constant flight Mach number of about 7.0 up to an altitude of 20 km. Thus, a measurement time of approx. 45 sec is available for measurements on hypersonic flow effects. The selected flight path fits rather well inside the operational range of the high enthalpy ground facilities of DLR, allowing numerical and ground base data correlations with flight measurements. From the mission point of view, the challenge of SHEFEX is the definition of a reentry configuration which has to fly aerodynamically stable without control surfaces and spin. Additionally, the time between the separation of the second stage and the initiation of the recovery sequence is very short (less than 20 sec). The second stage will separate just before deploying the parachute recovery system.

4. Applied Numerical Tools

The aerodynamic and aerothermodynamic studies are performed based on calculations with the DLR Euler- and Navier-Stokes Code TAU [10] applying unstructured grids. Additionally, for general parameter studies the DLR surface inclination method HOTSOSE [11] is applied. As shown in several comparisons with wind-tunnel experiments [12], [13] both codes are well established for the aerodynamic layout and analysis of complex space transportation systems. In all calculations perfect gas was assumed which is the worst case assumption from an engineering point of view.

5. Aerothermodynamic Studies

Main purpose of the aerothermodynamic analysis of the SHEFEX forebody was the assessment of the expected heatloads and a first analysis of the flow field. At the beginning an average flight Mach number of M=7.5 was assumed. Hence, the results represent the upper limit of the expected thermal loads. The calculations cover the complete Reynolds number range of $70.000 < Re < 3.500.000$. Dependent on the altitude the boundary layer is assumed to be fully laminar or fully turbulent. The wall was assumed to behave radiation adiabatic (ε=0.83). The analysis of the surface values of pressure, temperature and heat flux are basis for the choice of the flight instrumentation and the positioning of the sensors. Fig. 8 and Fig. 9 illustrate the influence of the boundary layer state on the flow field and the surface temperature. Although the forebody is very simple a complex and interesting flow field is obtained. In the backward part of the lower surface which is intended to simulate conditions of a deflected control surface parallel to the hinge line a separation is obtained which clearly decreases in case of a turbulent boundary layer. Additionally, the coloured streamlines show, that along the highly swept corner of the second forebody-segment a small vortex is obtained (see enlarged view). This vortex hits on the backward inclined panel and induces a local hotspot as shown in Fig. 9. To capture this phenomenon the number of sensors are increased in these regions (Fig. 10). The surface temperatures indicate that except of the unswept leading edge of the forebody never a critical tempature with view to the resilience of the ceramic panels is reached. The shown temperatures are a measure for the upper temperature limit because they represent the never obtained steady state conditions without taking into account the structural heat conductivity.

One critical point of the configuration is the step appearing between forebody and the first cylindrical segment (Fig. 11). Here, heat loads in the order of the ones at the unswept leading edge are expected. In any case structural failures due to thermal loads or shock-shock interactions have to be prevented because they would end in the destruction of the vehicle. Therefore, special emphasis is taken on the analysis of this region. The complex interaction between the separation induced shock and the forebody shocks is shown in Fig. 11. By comparison of the lines of constant Mach number and the pressure coefficients the slip line which might be critical with view to the heat loads can be detected. The analysis of this region was mainly performed based on 2D calculations of the symmetry plane. The validity of this assumption is given by the comparison of a 3D and a 2D surface temperature distribution along the lower surface of the forebody (Fig. 12). Fig. 13 shows that the separated hot boundary layer flow is redirected back into the separation bubble. This results in very high radiation adiabatic temperatures but it has to be taken into account that these results are steady state solutions and that the structural conductivity in neglected. A not fully coupled finite element calculation during the structural layout indicated that a material with high thermal conductivity, like copper, will be able to withstand the heatloads without total structural damage. If the high temperature area between slip line and shock is considered it is obvious that thermal loads coming from this region will not affect the surface flow for the flow conditions expected to appear during the SHEFEX experiment. Currently, additional Navier-Stokes calculations of the fin region are

under investigation which shall exclude severe problems resulting from shock-shock intercations and the corresponding hot spots.

6. Aerodynamic Layout of the Reentry Configuration

The layout of the reentry configuration is dominated by the lift of the asymmetric payload which drastically reduces the static margin. Additionally, the requirement of a stable atmospheric reentry differs from the conventional tumbling motion of the flat spinning payload that is usual for standard sounding rocket missions. The asymmetric shape of the SHEFEX payload and the resulting lift and pitching moment lead to a non zero trim angle. Main goal of the aerodynamic layout is the definition of a configuration which is stable with view to the longitudinal as well as the lateral motion. In order to reduce the drag as well as the structural loads the angle of attack has to be as close as possible to the originally projected angle of $\alpha \approx 1°$. Aggravating boundary conditions for the layout are, that the fins of the second stage must not be deflected and that the adaptation of overall center of gravity of the reentry configuration is very demanding due to the high mass of the burnt out engine. A first analysis of several fin arrangements with view to the static margin pointed out that only a four fin configuration with two horizontal and two vertical fins would enable to define a realistic reentry configuration. Additionally, the fins were defined as large as possible (red, Fig. 14). Here, the fin size is restricted by the ascent stability. For the estimated center of gravity at $x_S/l=0.4748$ even this configuration is unstable during the return flight. In order to obtain an acceptable angle of attack of $\alpha<3°$ it requires a center of gravity at $x_S/l=0.4$ which is not achievable with the possible margin of ballast. Therefore, a variety aerodynamic solutions to shift the center of pressure backward were assessed. Solutions like an increase of the fin size or an adaptation of the fin airfoil were not sufficient. Horizontal fins used as all flying rudders were very efficient but not realistic because a controlled vehicle would require a destroying system which is too expensive and too heavy. The only realistic aerodynamic change is the introduction of a flare in the back of the vehicle. A sensitivity study allowed to realize the best compromise between additional drag and increase of the static margin (flare564, Fig. 15). In combination with several structural changes to shift the center of gravity frontward and a light weight spacer in front of the Orion motor a first stable configuration was realized (Fig. 6). At this point it was sure that the planned mission at $\alpha=3°$ is feasible (Fig. 16). Unfortunately, the required ballast mass of 30kg reduced the apogee to only 280km for the given conditions. The resulting average flight Mach number was no more than M=6.6 which did not allow a direct comparison of flight measurements and HEG experiments. Therefore, due to the convenient static margin of the vehicle in a second design cycle the introduced spacer was left out resulting in a mass reduction of 16kg which, if required, might be partially used as ballast in the front part of the vehicle. The resulting final configuration is shown in Fig. 17. The corresponding pitching moment coefficients in Fig. 18 point out that the final vehicle will allow the projected maximal angle of attack of $\alpha \leq 3^{\circ}$. Additionally, the mass reduction enables an average Mach number of M≈7.

7. Layout of the Final Rocket System

Due to the aerodynamically required adaptation of the second stage a redesign of a large number of components was indispensable. The extensive structural adaptations on the second stage were the introduction of a flare and the resulting redesign of the fins. The fully symmetric fin arangement of the second stage which is required to prevent spin during descent forces also a redesign of the first stage fins and the corresponding tailcan (Fig. 19).

For the design of the flare, the standard boattail version of the tailcan (Fig. 5) has been taken as draft, concerning the total length and the distances of the four tailcan rings. The shims are connected with the four rings and provide the stiffness of the tailcan assembly. The aft ring consists of an outer ring and an inner ring that are connected with braces. The inner ring has the same inner diameter as the end ring of the standard boattail tailcan to apply the standard Improved Orion interstage adapter (Fig. 20). The structural layout of the flare and its structural optimization concerning mass and stiffness is performed applying ANSYS FEM analyses (Fig. 21).

The fins of the second stage had to be enlarged and adapted to the new flare. For the design of the fins, a concept that was already used for the development of the S30 fins. Instead of parallel rips in the fin frame, the rips spread from the aft corner of the trailing edge to the tip chord and leading edge. This leads to ideal force transportation and stress distribution. A CAD model of the fin is shown in (Fig. 22).

Unfortunately, these modifications of the reentry vehicle reduce the vehicle stability during ascent. Therefore, also for the first stage a new tailcan and fins had to be developed based on the original three fin configuration of the S30 motor. Aerodynamically, the new fins are similar to the ones of the second stage. But, the tailcan of the S30 had to be adapted to a four fin version because it exclusively has to enable the required spin for the ascent (Fig. 19). The structural layout was changed from an integral construction to a stringer and ring structure (Fig. 22 and Fig. 23).

The asymmetry of the SHEFEX experiment itself is no

problem during ascent as it is covered by an ogival nose cone (Fig. 5). The separation of the nose cone and the exclusion of a possible collisons with the SHEFEX experiment is guaranteed by a passive spring system (Fig. 19).
Due to the modification of the interstage section a passive spring system is also required in order to ensure the stage separation before ignition of the second stage. It consists of four springs with around 250 N maximum force each. These will provide ca. 5 m/s^2 additional relative acceleration between the two stages.

After the burnout of the S30 motor during the exoatmospheric ballistic trajectory, an Attitude Control System (ACS, Fig. 24) using cold gas thrusters, will remove any residual spin and perform a manoeuvre to provide a nominal zero degree angle of attack at the commencement of the re-entry phase of the trajectory and limited roll-control during the experiment phase (Fig. 25). An inertial platform, which is part of the autonomous service module, will measure the attitude and acceleration, calculate the instantaneous trajectory and provide the attitude control signals for the ACS. Experiment, attitude, acceleration and housekeeping data are transmitted via two redundant S-Band links and in addition stored onboard in a data recorder. Telecommand permits the in-flight reception by the ACS of discrete and serial commands from the ground.

Once the beginning of reentry is arrived the descent of SHEFEX will be much different to a usual flat spin reentry [14]. In comparison to a tumbling payload the SHEFEX vehicle produces much less drag and therefore, the deceleration will be much smaller. The main flight parameters during the experiment phase are shown in Fig. 26. The vehicle reaches Mach numbers from 6.4 to 7.3, respectively velocities from 1.95 km/s to 2.15 km/s during the experiment phase. The atmospheric influence gets important at an altitude of approximately 45 km and a significant increase of the dynamic pressure has to be taken account below 20 km. The experiment phase will end at an altitude of 20 km with the separation of the payload from the Improved Orion motor under hypersonic conditions. The payload module with the SHEFEX experiment will be highly unstable and will decelerate in a tumbling motion to a recovery velocity of approximately 230 - 280 m/s. At an altitude of 4 km the recovery sequence starts with the deployment of a two-stage parachute system to provide a final sink rate of approximately 15 m/s at water impact.

8. Conclusions

The purpose, the aerodynamic and structural layout and the projected mission of the SHEFEX flight experiment is introduced. SHEFEX does not deal with the design of a new reentry vehicle. It is a hypersonic experiment on a new concept for future aerospace vehicles which should have the potential to reduce cost and servicing efforts for the TPS and at the same time enhance vehicle performance due to the hypersonic exploitation of the aerodynamic sharp configuration concept. The main purpose of the flight experiment is the validation of analytical predictions, cross checking the ground testing data and acquisition of flight testing on some structural design features like sharp leading edges and seal system for the development of future space transportation systems. Designed following an unconventional way, is SHEFEX one of the first concepts resulting from a multidisciplinary approach. Finally, SHEFEX is a pathfinder project of an emerging strategy on a kind of sky based facility, as economical way to acquire knowledge in the physics of hypersonic flight.

The complete layout is based on Euler- and Navier-Stokes calculations applying the DLR TAU code on unstructured grids. The aerodynamic layout is dominated by the large amount of lift production of the asymmetric forebody which drastically reduces the static margin. A parameter study to increase the static margin by adaptation of the center of gravity leads to a final configuration with enlarged fins and a flare in the back of the reentry configuration. The changes allow a comfortable static margin and an average flight Mach number of M=7 at $\alpha \leq 3^{\circ}$. But, although the experiment is relatively simple at first view, the results of the aerodynamic requirements end in a nearly complete structural redesign of the applied typical sounding rocket combination consisting of a S30 motor as first stage and an Improved Orion motor as second stage.

9. References

1. Longo, J.M.A.; Püttmann, N.:
   The Sharp Edge Flight Experiment SHEFEX,
   Proceedings of the DGLR Jahrestagung, DGLR-2004-072, September 2004.

2. Longo, J.M.A.:
   Aerothermodynamics - A critical review at DLR,
   Aeosp. Sci. Technol. 7 (2003) 429-438.

3. AW&ST:
   Waverider Results,
   Aviation Week & Space Technology, November 10, 2003, pp. 17.

4. University of Queensland:
   A Description of the HyShot Experiment,
   www.uq.edu.au.

5. Kolodziej, P.; Bowles, J.V.; Roberts, C.:
Optimizing Hypersonic Sharp Body concepts from a Thermal Protection System Perspective,
AIAA Paper 98-1610,1998.

6. Strohmeyer, D.; Eggers, Th.; Haupt, M.:
Waverider Aerodynamics and Preliminary Design for Two-Stage-to-Orbit Missions, Part 1,
Journal of Spacecraft and Rockets, Vol. 35, No. 4, July-August 1998, pp. 450-458.

7. Eggers, Th.; Novelli, Ph.; Haupt, M.:
Design Studies of the JAPHAR Experimental Vehicle for Dual Mode Ramjet Demonstration,
AIAA Paper 2001-1921, 2001.

8. Reuther, J. et al.:
A Reusable Space Vehicle Design Study Exploring Sharp Leading Edges,
AIAA Paper 2001-2884, 2001.

9. Arnold, J.; Johnson, S.; Wercinski, P.:
SHARP: NASA's Research and Development Activities in Ultra-High Temperature Ceramic Nose Caps and Leading Edges for Future Space Transportation Vehicles,
Proceedings of the 52nd International Astronautical Congress, IAF paper 01-V.5.02, France, October 2001.

10. Mack, A.; Hannemann, V.:
Validation of the Unstructured DLR-TAU-Code for Hypersonic Flows,
AIAA Paper 2002-3111, 2002.

11. Reisch, U.; Anseaume, Y.:
Validation of the Approximate Calculation Procedure HOTSOSE for Aerodynamic and Thermal Loads in Hypersonic Flow with Existing Experimental and Numerical Results,
DLR-FB 98-23, 1998.

12. Eggers, Th.:
Longitudinal Stability and Trim of an Ariane 5 Fly-Back Booster,
AIAA Paper 2003-7055, 2003.

13. Tarfeld, F.:
Experimental Study on a Liquid Fly-Back Booster Configuration in Windtunnels,
AIAA Paper 2003-7056, 2003.

14. Stamminger, A.; Turner, J.; Hörschgen, M.; Jung, W.:
Sounding Rockets as a Real Flight Platform for Aerothermodynamic CFD Validation of Hypersonic Flight Experiments,
5th European Symposium on Aerothermodynamics for Space Vehicles, Cologne, Nov. 2004.

8. Figures

Fig. 1 The ARD capsule

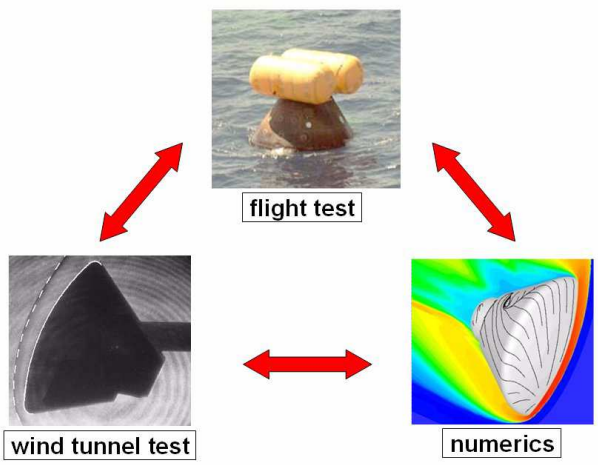

Fig. 2 Sources of aerodynamic data, example: ARD

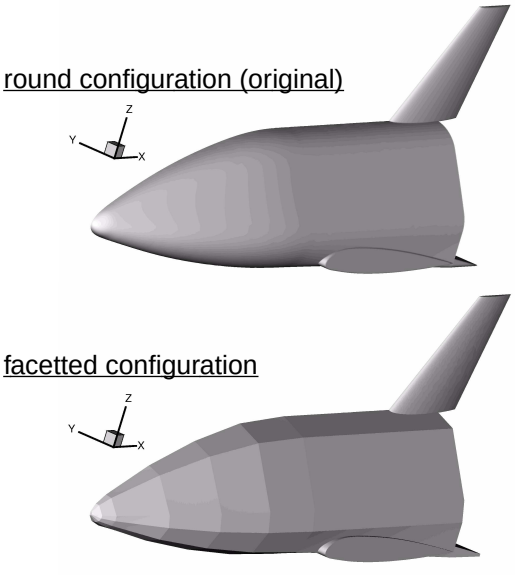

Fig. 3 Generic aerospace vehicles

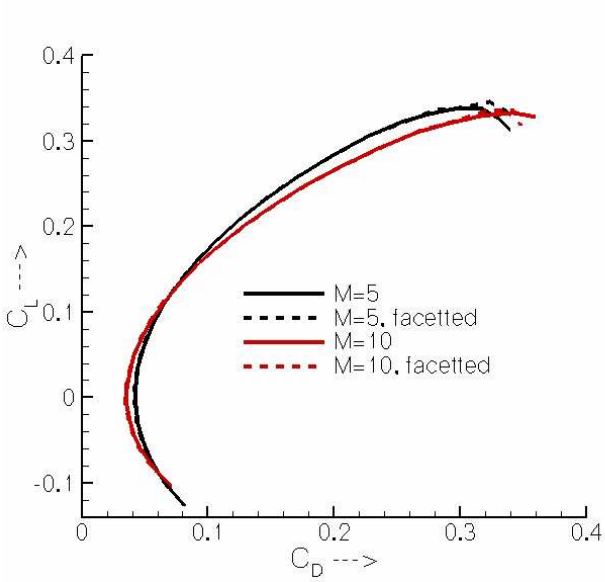

Fig. 4 Influence of the facetted surface on C_L and C_D

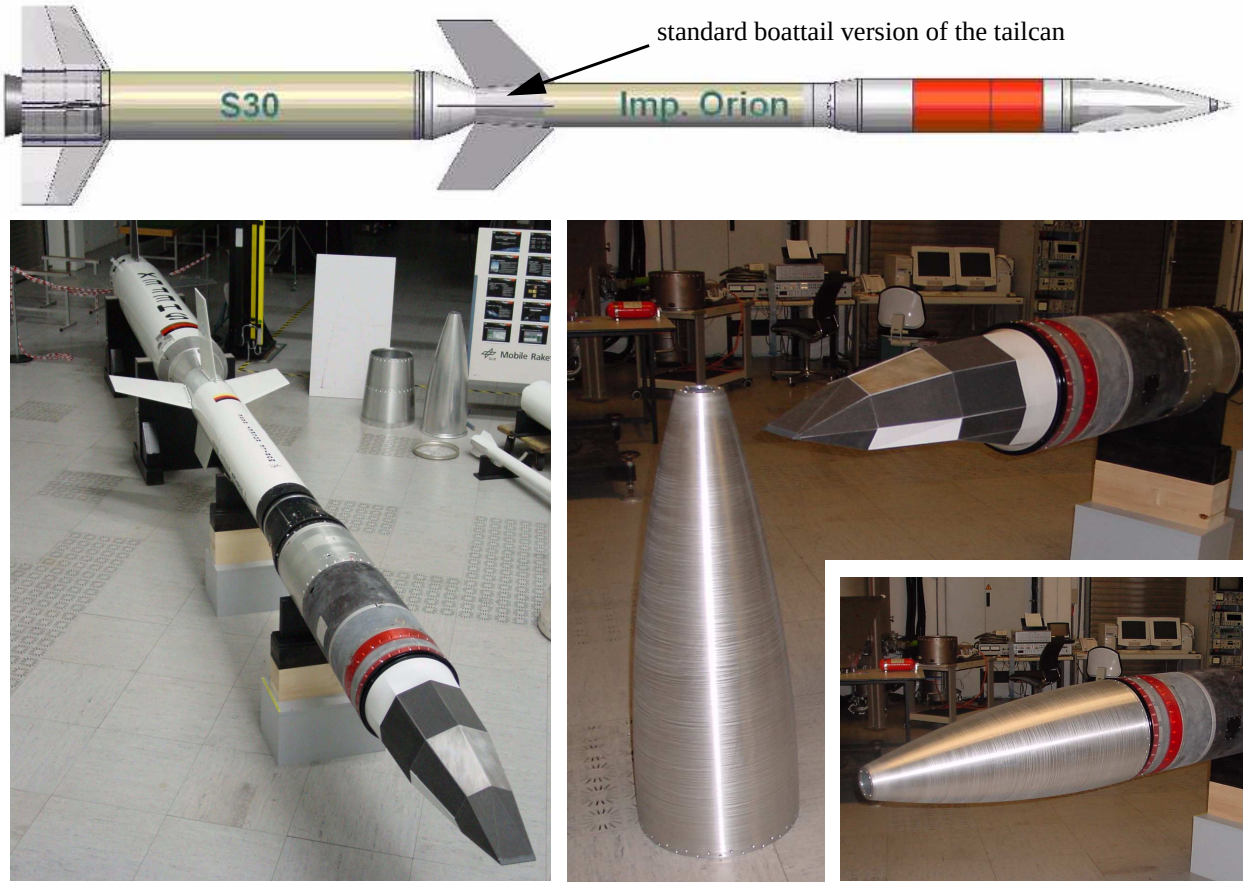

Fig. 5 Mock-up of the SHEFEX launch system

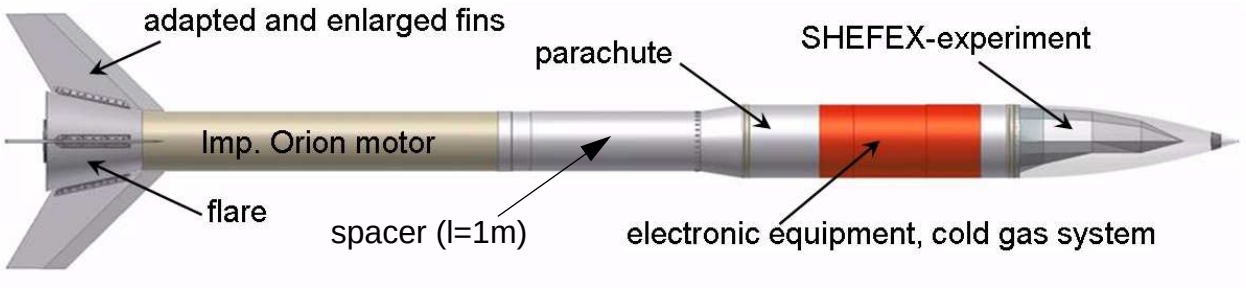

Fig. 6 SHEFEX reentry configuration

Time [sec]	Altitude [km]	Action
t_0	0	1st stage ignition and vehicle lift-off
t +28	17.5	1st stage burnout and stage separation
t +30	19.0	2nd stage ignition
t +56	65.5	2nd stage burnout
t +68	90.0	Nosecone separation
t +70	95.0	Start of ACS pointing maneuver
t +297	327.0	Apogee
t +528	90.0	Start of SHEFEX experiment phase
t +560	20.0	End of SHEFEX experiment phase
T +561	18.0	2nd stage separation
T +570	6.8	Start of recovery sequence

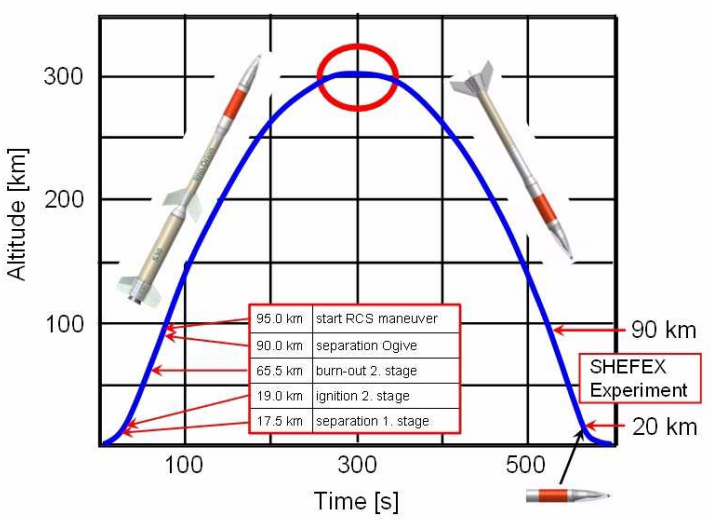

Fig. 7 SHEFEX mission procedure

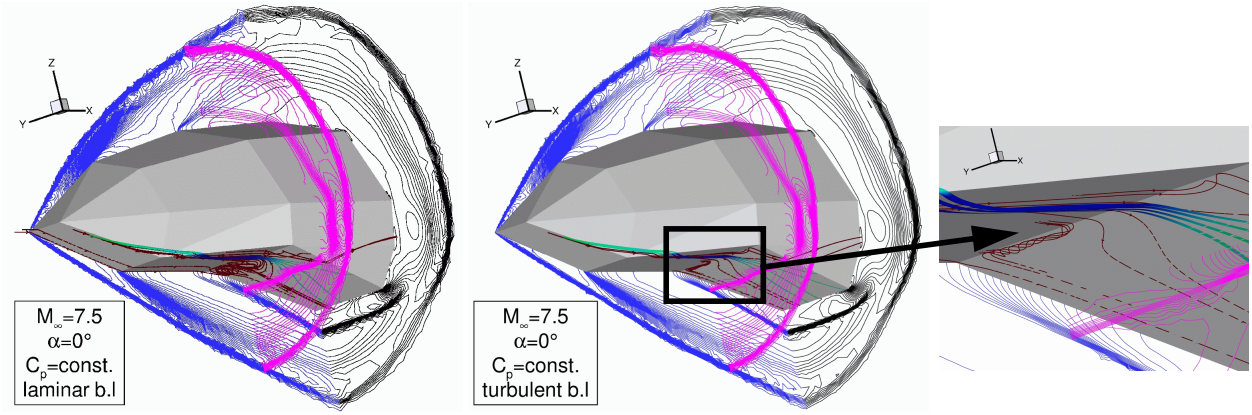

Fig. 8 Influence of the boundary layer state on the flow field, H=42.6 km

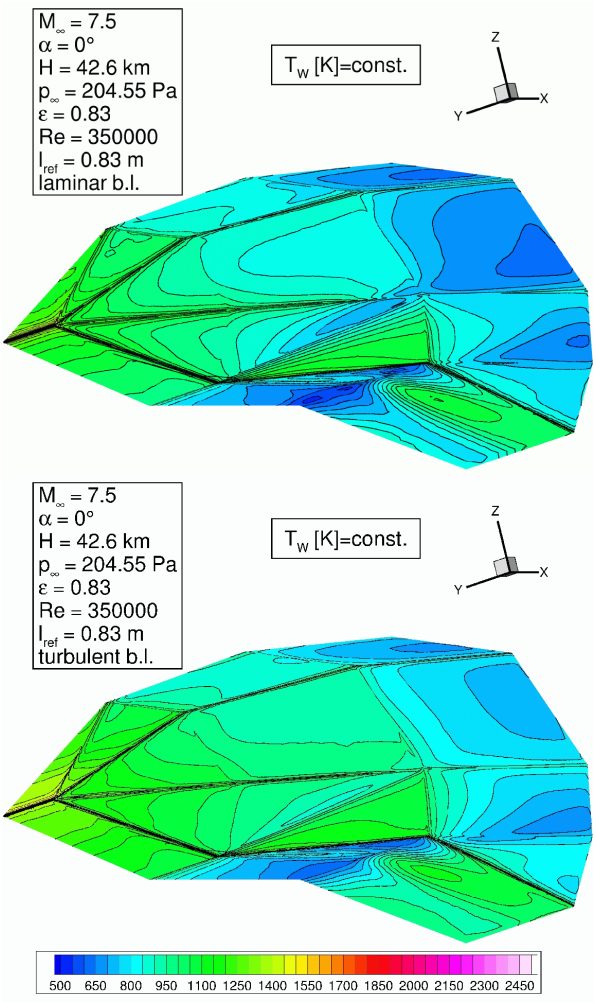

Fig. 9 Influence of the boundary layer state on the surface temperature, H=42 km

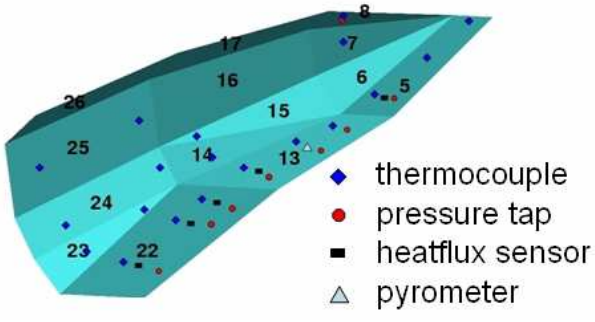

Fig. 10 Sensor positions on the SFEFEX forebody

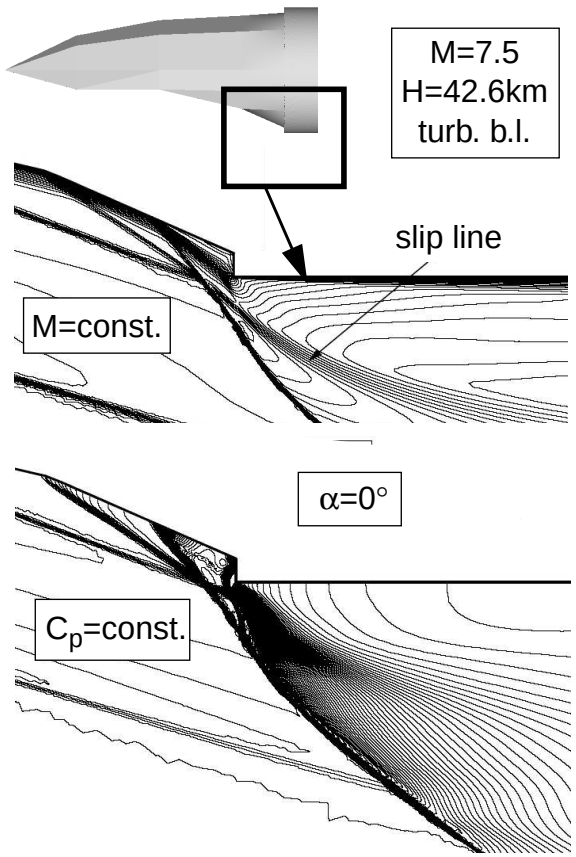

Fig. 11 Flow topology in symmetry plane

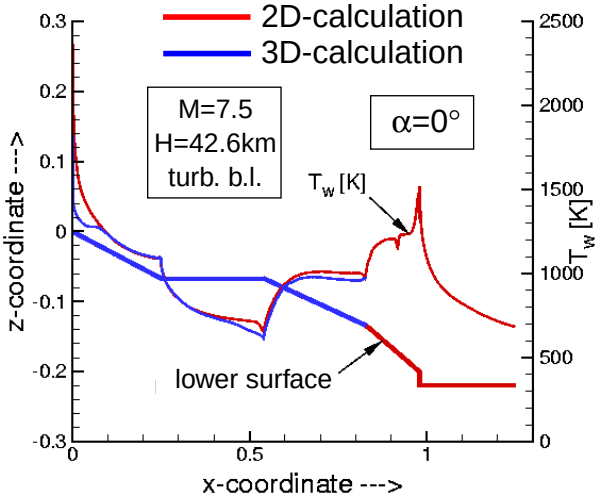

Fig. 12 Surface temperatures, 2D- and 3D-results

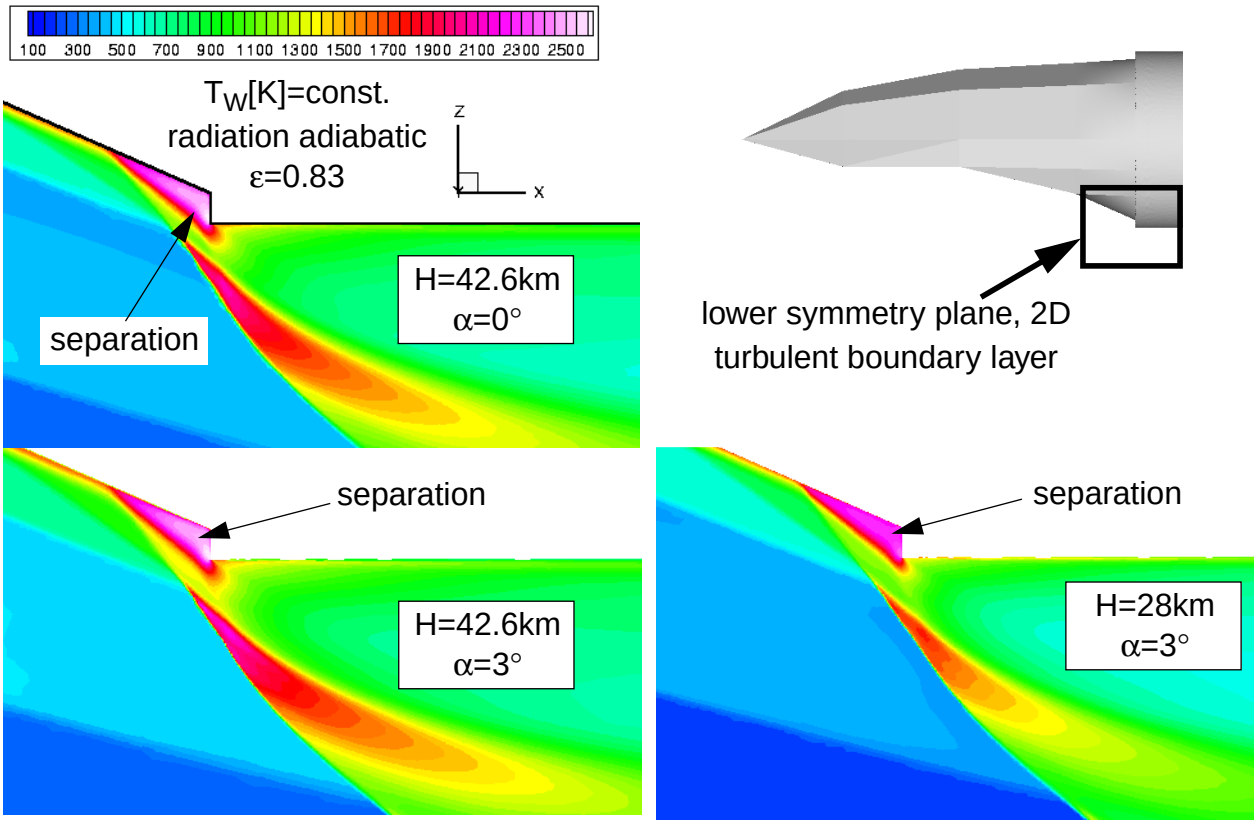

Fig. 13 Influence of angle of attack and altitude on the temperature

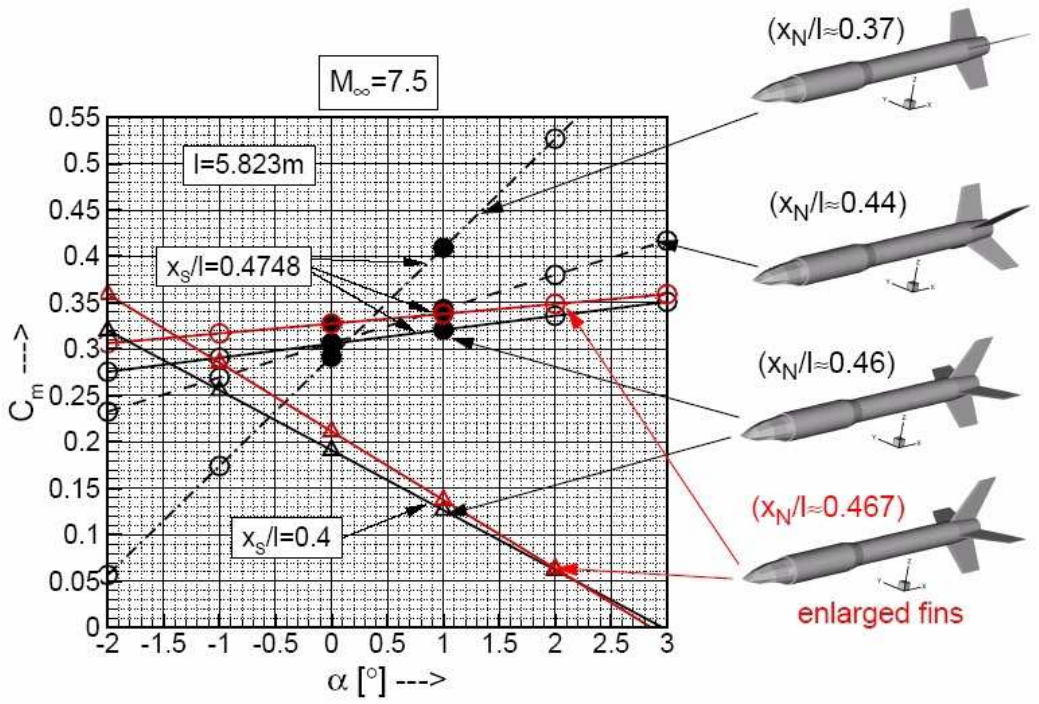

Fig. 14 Influence of fin number, fin position and fin size on the longitudinal stability

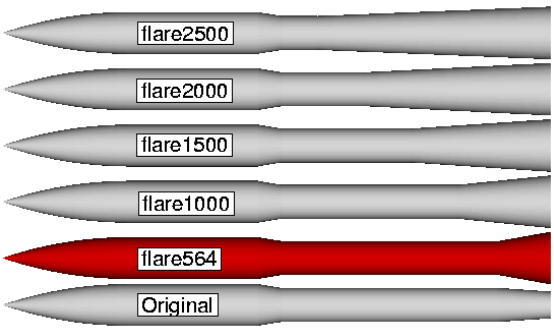

Fig. 15 Investigated flare geometries

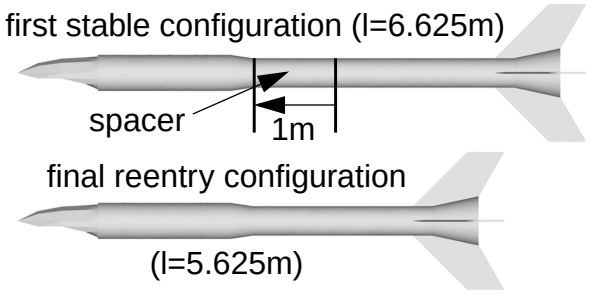

Fig. 17 Comparison of "new" and final vehicle

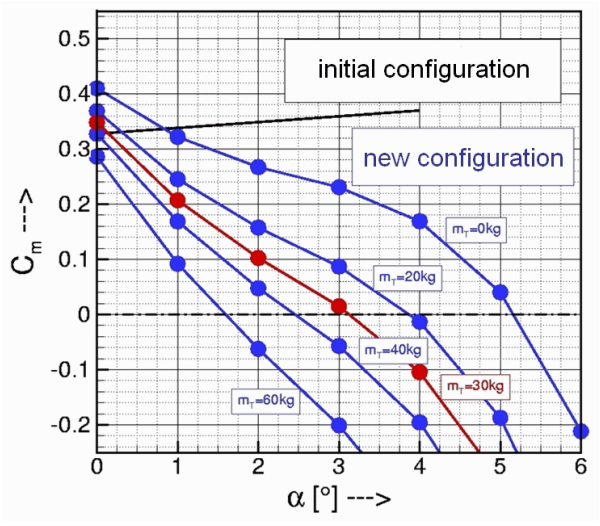

Fig. 16 C_m coefficients of the configuration with flare

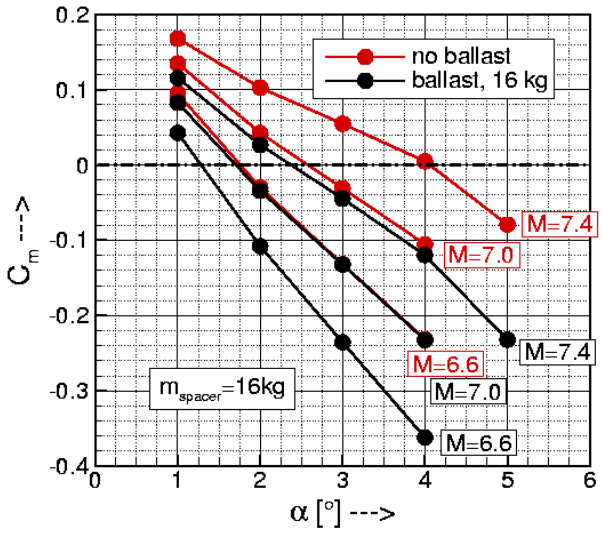

Fig. 18 C_m coefficients of the final configuration

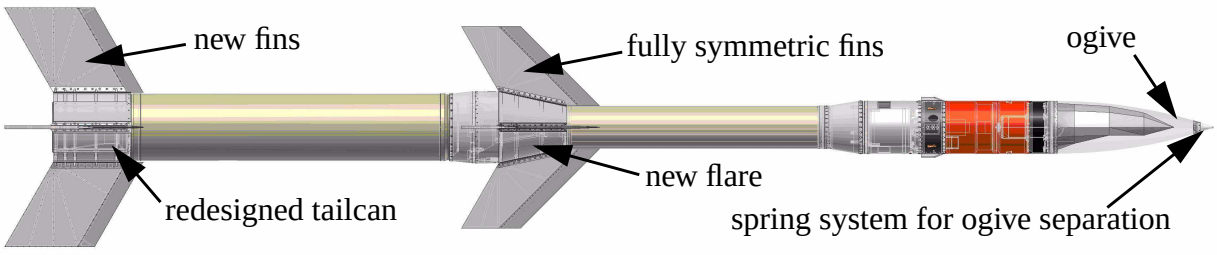

Fig. 19 Final SHEFEX rocket arrangement

Fig. 20 Flare without and with cladding

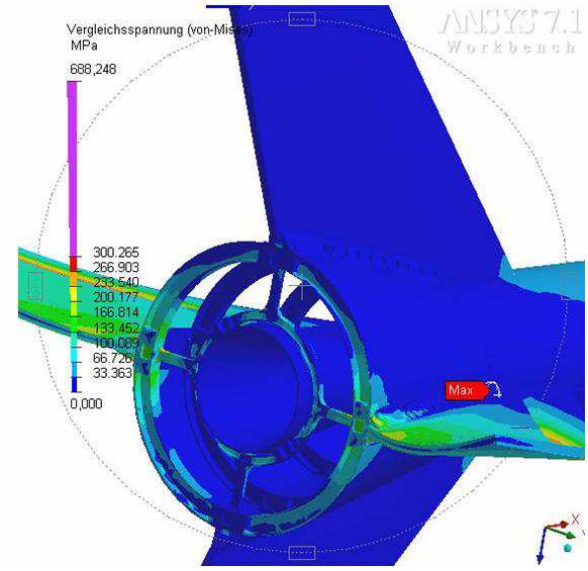

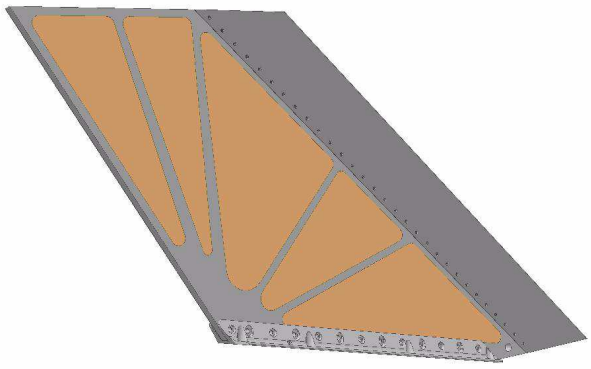

Fig. 22 CAD model of the fin structure, second stage

Fig. 21 FEM analysis of flare and fin, second stage

Fig. 23 Fin and tailcan of the S30 motor (first stage)

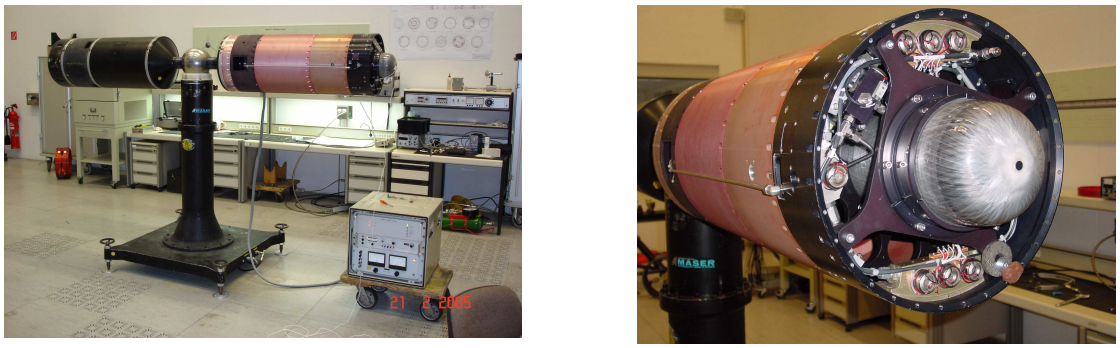

Fig. 24 ACS system on an air bearing test facility

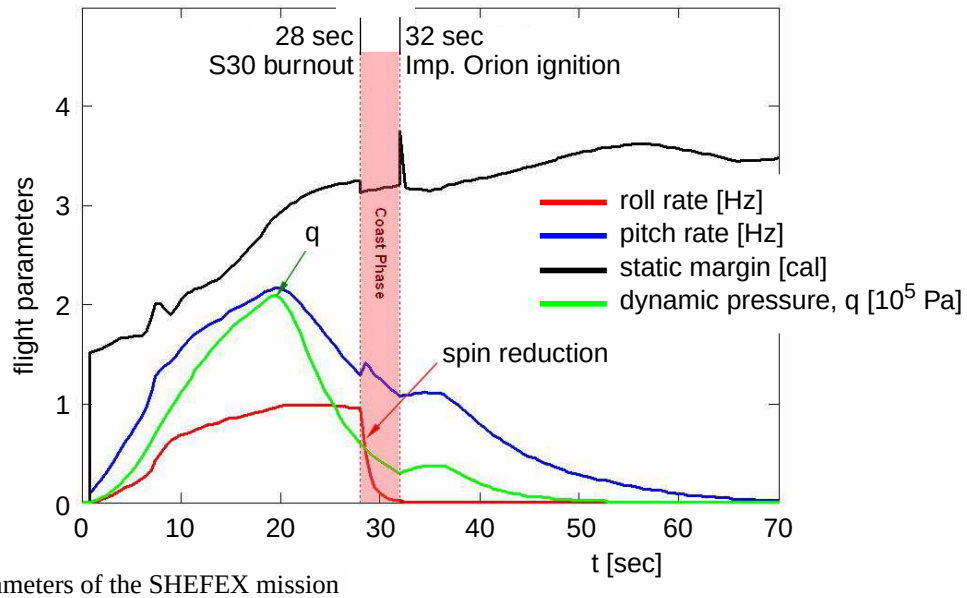

Fig. 25 Ascent parameters of the SHEFEX mission

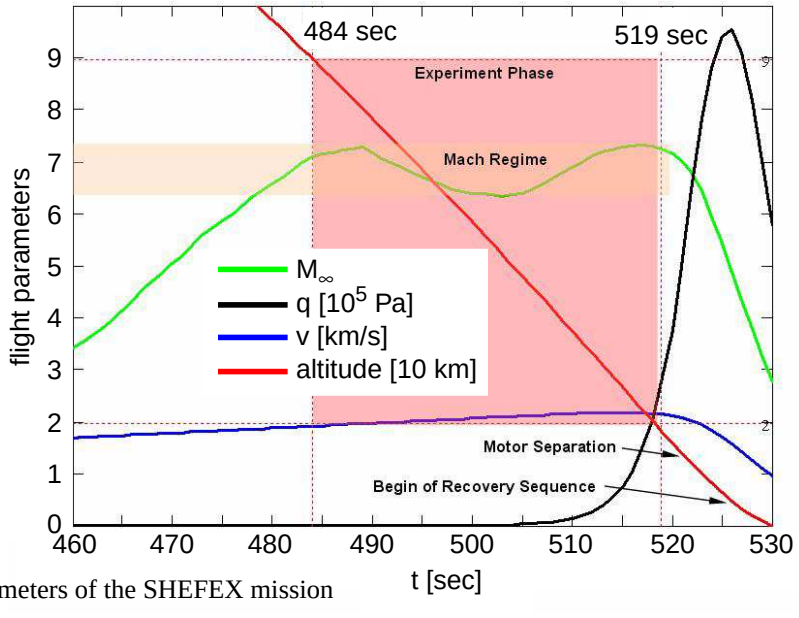

Fig. 26 Reentry parameters of the SHEFEX mission